AIP Journal of Applied Physics

Dynamic modeling of the behavior of permalloy for magnetic shielding

Z. Sun, M. Reisner, P. Fierlinger, A. Schnabel, S. Stuiber, and L. Li

Citation: Journal of Applied Physics **119**, 193902 (2016); doi: 10.1063/1.4949516
View online: http://dx.doi.org/10.1063/1.4949516
View Table of Contents: http://scitation.aip.org/content/aip/journal/jap/119/19?ver=pdfcov
Published by the AIP Publishing

Dynamic modeling of the behavior of permalloy for magnetic shielding

Z. Sun,[1,2,a)] M. Reisner,[3,b)] P. Fierlinger,[3] A. Schnabel,[2] S. Stuiber,[3] and L. Li[1]
[1]*Department of Electrical Engineering, Harbin Institute of Technology, 150001 Harbin, China*
[2]*Physikalisch-Technische Bundesanstalt Berlin, 10587 Berlin, Germany*
[3]*Physikdepartment, Technische Universität München, D-85748 Garching, Germany*

(Received 24 February 2016; accepted 2 May 2016; published online 17 May 2016)

The minimization of the remanent magnetization of ferromagnetic materials is a prerequisite for a reproducible low magnetic field inside shields. To realistically describe this so-called magnetic equilibration procedure, this paper proposes two approaches for the calculation of time- and space-dependent fields in the presence of ferromagnetic materials like permalloy. The first method is based on the Jiles-Atherton model and also takes into account frequency dependent effects. The second method is the newly developed empirical phase shift model, tailored specially for the simulation of the equilibration procedure. Both approaches are compared to experimental tests and show good quantitative agreement. *Published by AIP Publishing.*
[http://dx.doi.org/10.1063/1.4949516]

I. INTRODUCTION

Ultra-low magnetic fields below 0.5 nT and gradients below 0.1 nT/m are crucial for precise next generation experiments in fundamental research at low energies. This includes experiments which utilize spin-clocks or other nuclear magnetic resonance (NMR) methods to explore the laws of nature relevant in the early universe[1,2] beyond the reach of physics with accelerators and beyond the standard model of particle physics. NMR experiments using Ramsey's method of separated oscillatory fields are among the most precise measurements in physics,[3,4] e.g., searching for the electric dipole moment (EDM) of the neutron.[5] The next generation imposes even more stringent requirements on the magnetic environment as a prerequisite for stable and systematically clean operation. The currently best magnetically shielded rooms (MSRs) are the BMSR-2 at the Physikalisch-Technische Bundesanstalt in Berlin, damping external magnetic fluctuations by approximately 2×10^6 at 10 mHz,[6,7] and the recently built MSR at the Technische Universität München (TUM) with a damping factor of more than 10^6 at 1 mHz in a smaller space.[8,9]

The residual magnetic field inside a strong MSR is not only determined by the shielding factor but can also be dominated by the magnetization state of the materials used for shielding. The walls of an MSR are typically made of permalloy, a type of ferromagnetic material with high permeability. The remanent magnetization of the permalloy itself has an effect on the residual magnetic field, even if the external field is shielded quite well. In order to eliminate the magnetization, an alternating field with decreasing amplitude is applied to the material. As a result, the hysteretic curve spirals inwards and the magnetization decreases every cycle until the remaining field is quite small.[10] If it is done in a zero magnetic field environment, this process is known as demagnetization or degaussing. In the presence of a non-zero magnetic field, "equilibration" is a more appropriate name for this process, as the magnetic domains reach an optimum configuration in equilibrium within the background field.[11]

The BMSR-2 in Berlin features a residual field below 500 pT in a central volume of 1 m^3 after equilibration. This MSR with 7 layers of permalloy and 1 layer of aluminum provides a passive shielding factor of 75 000 at 10 mHz.[6,7] The outer shield of the MSR in TUM achieves a field of (700 ± 200) pT within a central volume of 1 m^3 after equilibration, while the 2 layers of permalloy and 1 layer of aluminum have a passive shielding factor of 300 at frequencies less than 10 mHz.[8] The similar residual field at the TUM-MSR is due to a revised equilibration system and clearly demonstrates that the residual field can be improved independently of the shielding factor.

The optimization of the equilibration processes is a complex problem even in the MSRs in Berlin and Munich. The residual field is dependent on the details of the equilibration process, such as the maximum field value, the envelope function of the decreasing field, the sequence, and the spacial arrangement of the field coils. In the past, the optimization relied on an iterative process which was solely based on empirical evidence and lacked effective theoretical guidance on optimal parameters. This paper presents two numerical methods for the calculation of the equilibration process. The first method is based on the Jiles-Atherton (JA) model, an established description of hysteretic behavior. The second method is a new model based on the phase shift between field strength and flux density of a material during equilibration. Both methods are discussed and the calculation results are compared to experimental measurements.

II. EQUILIBRATION CALCULATION BASED ON THE JA MODEL

The JA model describes the hysteretic behavior based on the analysis of the energy changes of magnetic domains during magnetization.[12–14] In this theory, an ideal state

a)Electronic mail: sunzhiyin1990@163.com
b)Electronic mail: Maximilian-Reisner@web.de

without impurities is represented by the anhysteretic magnetization M_{an}, approximated by a Langevin function. The magnetization M is composed of an irreversible component M_{irr} and a reversible component M_{rev}, related to M_{an}. M_{irr} can be obtained from the energy equation, in which the energy in the ideal case is equal to the magnetostatic energy plus the dissipated loss due to pinning sites. M_{rev} corresponds to the reversible domain wall bending during field changes.

The equilibration calculation method proposed in this paper uses the frequency dependent JA model[15,16] according to the vectorization concept.[17] Furthermore, the time dependence of the differential equations has been added. M_{irr} is solved by a differential equation depending on the effective field H_e, while M_{rev} is linearly dependent on the difference between M and M_{irr}. The method is represented by the following set of differential equations:

$$\frac{\partial \vec{M}}{\partial t} = (1-c)\frac{\partial \vec{M}_{irr}}{\partial t} + c\frac{\partial \vec{M}_{an}}{\partial t}, \tag{1}$$

$$\vec{M}_{an} = M_s\left(\coth\frac{|\vec{H}_e|}{a} - \frac{a}{|\vec{H}_e|}\right)\frac{\vec{H}_e}{|\vec{H}_e|}, \tag{2}$$

$$\vec{H}_e = \vec{H} + \alpha\vec{M}, \tag{3}$$

$$\vec{M}_{rev} = c(\vec{M}_{an} - \vec{M}_{irr}), \tag{4}$$

$$\frac{\partial \vec{M}_{irr\_dc}}{\partial t} = g\left(\frac{\vec{M}_{rev}}{ck}\frac{\partial \vec{H}_e}{\partial t}\right)\frac{\vec{M}_{rev}}{|\vec{M}_{rev}|}, \tag{5}$$

$$\frac{\partial \vec{M}_{irr\_ac}}{\partial t} = g\left\{\frac{\vec{M}_{rev}}{ck}\frac{\partial \vec{H}_e}{\partial t} - \frac{1}{\delta k(1-c)}\left[\frac{\mu_0 d^2}{2\rho\beta}\left(\frac{d\vec{M}}{dt}\right)^2 + \left(\frac{\mu_0 G d w H_0}{\rho}\right)^{\frac{1}{2}}\left(\frac{d\vec{M}}{dt}\right)^{\frac{3}{2}}\right]\right\}\frac{\vec{M}_{rev}}{|\vec{M}_{rev}|}, \tag{6}$$

where M_s is the saturated magnetization, a is the domain wall density, α is a mean field parameter representing the coupling of domains, k is the average energy required to break a pinning site, c is the coefficient of M_{rev}, ρ is the resistivity, β is a geometrical factor, d and w are the cross-sectional dimensions of the material, G is a dimensionless constant, and H_0 represents the fluctuating internal potential. $g(x) = x$ if $x \geq 0$ and $g(x) = 0$ if $x < 0$.

To simulate the equilibration process of a 3D object, the JA model is combined with the Finite Element Method (FEM). After building an arbitrary geometry in FEM software, the domain of permalloy is defined by setting the magnetization into the constitutive relations. The magnetization M is solved from the above equations using the partial differential equations (PDEs) interface in COMSOL, a commercial FEM software.

For instance, 3 cycles of an alternating field with linear decreasing envelope function as in Fig. 1(a) are applied to the excitation coil wound around a cylindrical piece of permalloy (Fig. 6(a)). An equilibration curve is calculated based on Eqs. (1)–(5), not including frequency dependence. A 10 Hz equilibration curve is calculated based on Eqs. (1)–(4) and (6), considering eddy current loss and anomalous loss

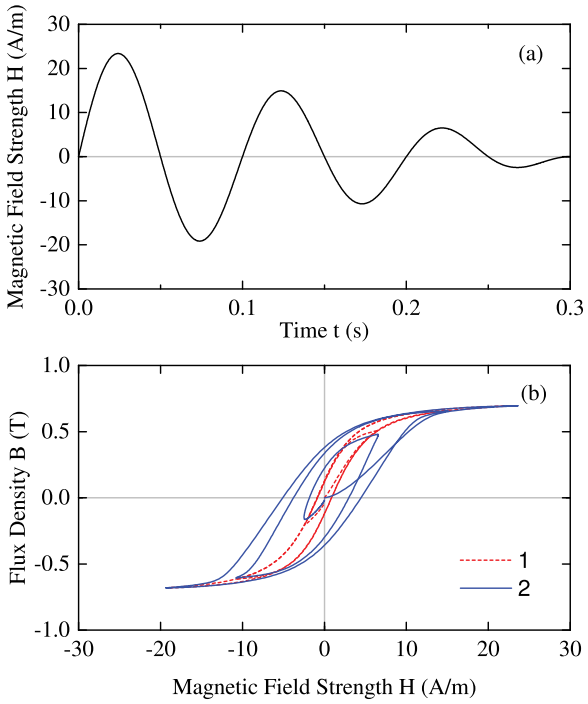

FIG. 1. (a) Applied field strength; (b) equilibration curves calculated based on the JA model not including frequency dependence (curve 1) and considering frequency dependence (curve 2). The parameters for the JA model are $M_s = 6 \times 10^5$ A/m, $a = 1.8$ A/m, $\alpha = 1 \times 10^{-6}$, $k = 2$ A/m, $c = 0.5$, $\rho = 1 \times 10^{-5}$ Ω m, $\beta = 16$, $d = 1$ mm, $G = 0.1356$, $w = 3$ cm, $H_0 = 0.0075$ A/m.

during hysteretic loops. The magnetic field in conductive ferromagnetic materials is impeded by the induced field of eddy currents. As a result, the field in the middle of the permalloy material is less than near the surface. Therefore, the average equilibration curve is wider and more elliptical depending on the conductivity of the material and frequency of the applied field.

The JA model permits the calculation of flux density changes induced by magnetic fields with arbitrary behavior in space and time. The practically interesting case of a decreasing alternating field H with a field offset is shown in Fig. 2. The applied background field is in the tangential direction relative to the radius of the cylindrical permalloy during equilibration. It is applied by an offset current through the excitation coil. The field H increases linearly from 0 to the offset value of 2 A/m within 0.1 s (Fig. 2(a)), leading to changes of B along the initial magnetization curve (Fig. 2(b)). While without the additional field the final point of the equilibration cycles approaches B close to 0 for $H = 0$ ((Fig. 1(b)), the new final point is located on the anhysteretic curve M_{an} with 2 A/m as the horizontal coordinate. The anhysteretic curve means that the material is in the state of the lowest potential energy after equilibration. Therefore, this calculated curve demonstrates how the material arrives at the optimal state during the equilibration process.

This simulation method based on the JA model is suitable for realistic simulations of magnetic shields equilibrated in the Earth's field and other environmental fields. Under these conditions, the background field varies in different positions of the geometry, resulting in different equilibration curves. All equilibration curves with infinite cycles terminate

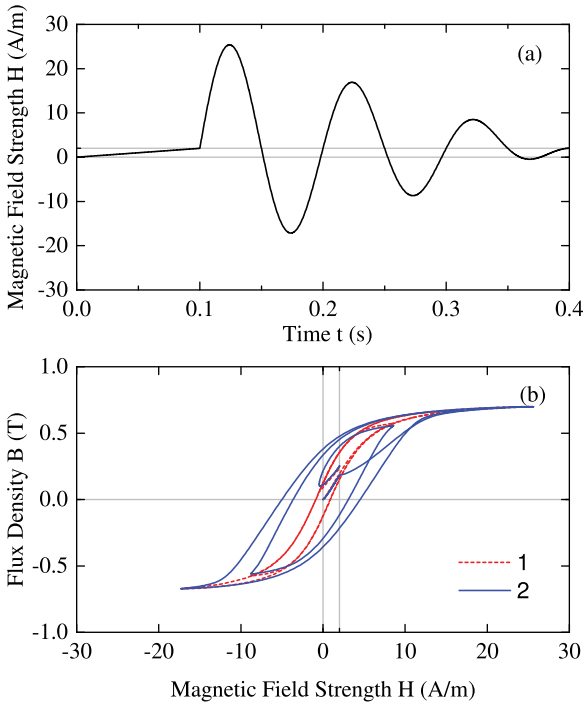

FIG. 2. (a) Same field as Fig. 1 but with 2 A/m field offset applied within the first 0.1 s; (b) equilibration curves with 2 A/m field offset, parameters, and curve descriptions as in Fig. 1.

at points on the anhysteretic curve with different horizontal coordinates. The whole material reaches an equilibrated state.

III. EQUILIBRATION CALCULATION USING THE NEW PHASE SHIFT MODEL

The disadvantage of the method based on the JA model is that its simulation requires the solution to several differential equations which results in significant computation time. A simplified model was created to be faster and was dubbed the phase shift model. It is a mathematical model which specifically simulates the equilibration process rather than describing hysteretic behavior by parameters with physical meanings. Typical magnetic flux B and magnetic field H values during demagnetization are shown in Fig. 3. It is found that there is a phase shift φ between B and H due to hysteresis and a time-dependent ratio of B to H due to saturation.

The phase shift model is based on the above two characteristics observed in experiments. It is restricted to fields of the type

$$H(t) = H_0 \cdot f(t) \cdot \sin(\omega t), \tag{7}$$

where $f(t)$ is an envelope function modulating the amplitude of the periodic alternating field.

The flux density B should be a sinusoidal function with a phase shift and a variable amplitude

$$B(t) = B_0 \cdot f\left(t - \frac{\varphi}{\omega}\right) \cdot \sin(\omega t - \varphi). \tag{8}$$

In the magnetic fields interface of COMSOL's AC/DC module, the vector potential $\vec{A}$ is the dependent variable. The phase shift model is constructed using the relation

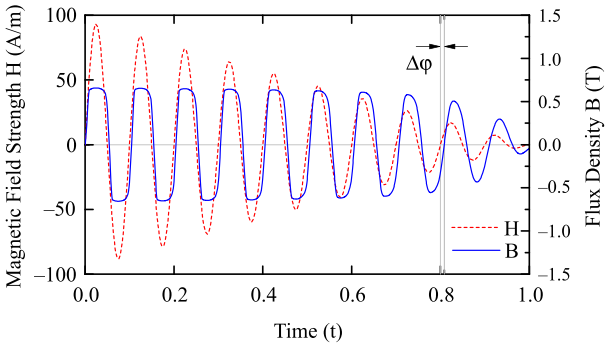

FIG. 3. $H(t)$ and $B(t)$ during demagnetization.

$$\nabla \times \vec{A} = \vec{B} = \mu_0(\vec{H} + \vec{M}). \tag{9}$$

Instead of dealing with $\vec{M}$ dependent on $\vec{H}$, $\vec{M}$ dependent on $\vec{B}$ at one point in one direction is derived

$$\begin{aligned}
M &= \frac{B_0}{\mu_0} f\left(t - \frac{\varphi}{\omega}\right)\sin(\omega t - \varphi) - H_0 f(t)\sin(\omega t) \\
&= \frac{B_0}{\mu_0} f\left(t - \frac{\varphi}{\omega}\right)\sin(\omega t - \varphi) \\
&\quad - H_0 f(t)\left[\sin(\omega t - \varphi)\cos(\varphi) + \cos(\omega t - \varphi)\sin(\varphi)\right] \\
&= \left[\frac{B_0}{\mu_0} f\left(t - \frac{\varphi}{\omega}\right) - H_0 f(t)\cos(\varphi)\right]\sin(\omega t - \varphi) \\
&\quad - \frac{H_0 f(t)\sin(\varphi)}{B_0 \omega f\left(t - \frac{\varphi}{\omega}\right)}\left[\frac{dB(t)}{dt} - B_0 \frac{df\left(1 - \frac{\varphi}{\omega}\right)}{dt}\sin(\omega t - \varphi)\right] \\
&= B_0 f\left(t - \frac{\varphi}{\omega}\right)\sin(\omega t - \varphi)\left[\frac{1}{\mu_0} - \frac{H_0 f(t)\cos(\varphi)}{B_0 f\left(t - \frac{\varphi}{\omega}\right)}\right. \\
&\quad \left. + \frac{H_0 f(t)\sin(\varphi)}{B_0 \omega f^2\left(t - \frac{\varphi}{\omega}\right)} \frac{df\left(1 - \frac{\varphi}{\omega}\right)}{dt}\right] - \frac{H_0 f(t)\sin(\varphi)}{B_0 \omega f\left(t - \frac{\varphi}{\omega}\right)} \frac{dB(t)}{dt}.
\end{aligned} \tag{10}$$

To establish the ratio of B to H, a variable $\mu(B)$ is defined as

$$\mu(B) = \mu_0 \mu_r(B) = \frac{B_0}{H_0}. \tag{11}$$

Then, the magnetization M becomes

$$\begin{aligned}
M &= \left[1 - \frac{\omega F(t)\cos(\varphi)}{\mu_r} + \frac{F(t)\sin(\varphi)}{\mu_r f\left(t - \frac{\varphi}{\omega}\right)} \frac{df\left(t - \frac{\varphi}{\omega}\right)}{dt}\right] \frac{B(t)}{\mu_0} \\
&\quad - \frac{F(t)\sin(\varphi)}{\mu_0 \mu_r} \frac{dB}{dt}(t),
\end{aligned} \tag{12}$$

where $F(t) = \frac{f(t)}{\omega f(t - \frac{\varphi}{\omega})}$.

The above equations are generalized for 3D simulations in COMSOL. By implementing M in Eq. (12), the solved B

has a phase shift to H and field dependent amplitude related to μ_r. When $f(t)$ is a linear decreasing function, an ellipsoidal-shaped spiral curve can be obtained. By changing the function $\mu_r(B)$, equilibration curves with different hysteretic parameters can be simulated. Note that, for anisotropic ferromagnetic materials, μ_r can be set as $\mu_r(B_x, B_y, B_z)$. Fig. 4 shows the equilibration curves obtained with a constant μ_r and a nonlinear $\mu_r(B)$ which creates saturation behavior. To describe the behavior of permalloy, $\mu_r(B)$ is fitted to equilibration curve measurements. To achieve a symmetric behavior with respect to B, an even polynomial function is chosen for $\mu_r(B)$ as a continuous and differentiable function

$$\mu_r(B) = \mu_{max} + \sum_{i=1}^{N} v_i B^{2i}, \tag{13}$$

where the parameters v_1 and v_2 are chosen in a way that $\mu_r(B)$ smoothly decreases at saturation

$$v_1 = 2\frac{1-\mu_{max}}{(\mu_0 M_s)^2} + \sum_{i=3}^{N}(i-2)v_i(\mu_0 M_s)^{2(i-1)}, \tag{14}$$

$$v_2 = \frac{\mu_{max}-1}{(\mu_0 M_s)^4} - \sum_{i=3}^{N}(i-1)v_i(\mu_0 M_s)^{2(i-2)}. \tag{15}$$

N was chosen to be 6, which is sufficiently large for our purpose.

To incorporate additional ambient fields into the equilibration procedure, M is re-derived with a slightly different ansatz

$$M = \left(1 - \frac{\omega F(t)}{\mu_r(B)}\cos(\varphi) + \frac{\tilde{F}(t)}{\mu_r(B)}\sin(\varphi)\right)\frac{B-B_a}{\mu_0} - \frac{F(t)}{\mu_0\mu_r(B)}\sin(\varphi)\frac{d(B-B_a)}{dt} + M_a(H_a), \tag{16}$$

where $M_a = \frac{B_a(t)}{\mu_0} - H_a(t)$. $H_a(t)$ and $B_a(t)$ are time-dependent but quasi-static ambient fields. The fields H_a and B_a are typically set according to the additional static field. An equilibration curve based on this model is shown in Fig. 5.

As an improvement of the model, the energy to overcome the pinning sites is taken into account by a time dependent phase shift $\varphi(t)$

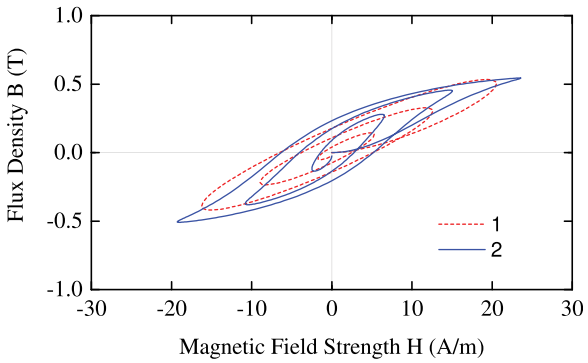

FIG. 4. Equilibration curves using the phase shift model with a constant $\mu_r = 20\,000$ (curve 1) and a nonlinear $\mu_r(B)$ (curve 2) with parameters: $\mu_{max} = 40\,000$, $\mu_0 M_s = 0.73\,\mathrm{T}$, $v_3 = -13\mu_{max}\,\mathrm{T}^{-6}$, $v_4 = -30\mu_{max}\,\mathrm{T}^{-8}$, $v_5 = 42\mu_{max}\,\mathrm{T}^{-10}$, $v_6 = 15\mu_{max}\,\mathrm{T}^{-12}$.

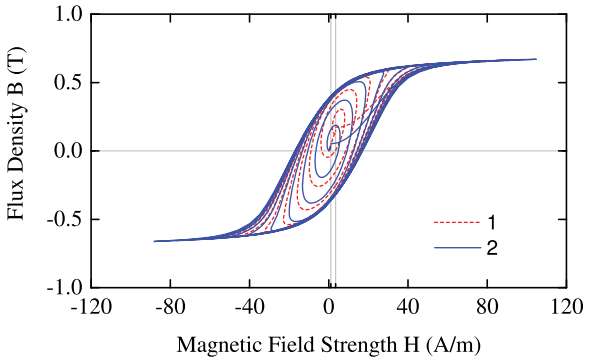

FIG. 5. Equilibration curves with 1 A/m offset (curve 1) and 3 A/m offset (curve 2) with the same parameters as curve 2 in Fig. 4.

$$\varphi(t) = \varphi_0(1 + c_1 t + c_2 t^2), \tag{17}$$

where the parameters c_1 and c_2 are chosen to match experiments.

IV. EXPERIMENTS

For validation of the simulations, a cylindrical sample of permalloy (Magnifier^{R}7904) with 1 mm thickness, 3 cm width, and 10 cm diameter as shown in Fig. 6(a) was tested.

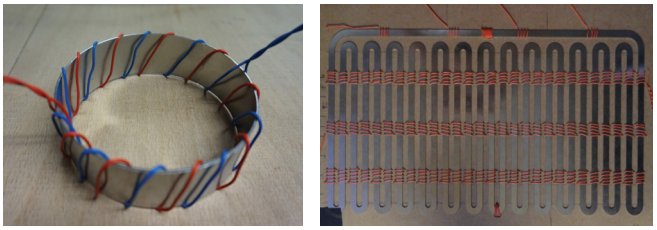

FIG. 6. (a) The cylindrical sample and (b) the snake sample.

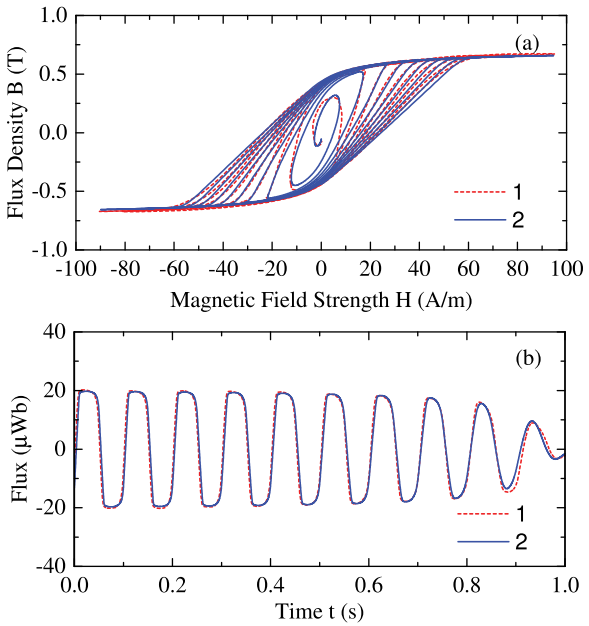

FIG. 7. (a) Measured (curve 1) and calculated (curve 2) equilibration curves based on the JA model; (b) measured (curve 1) and calculated (curve 2) flux. The fitted parameters are $M_s = 5.5 \times 10^5$ A/m, $a = 5$ A/m, $\alpha = 1.5 \times 10^{-5}$, $k = 2.4$ A/m, $c = 0.9$, $\sigma = 6 \times 10^5$ S/m, $\beta = 16$, $d = 1$ mm, $G = 0.1356$, $w = 3$ cm, and $H_0 = 0.0075$ A/m.

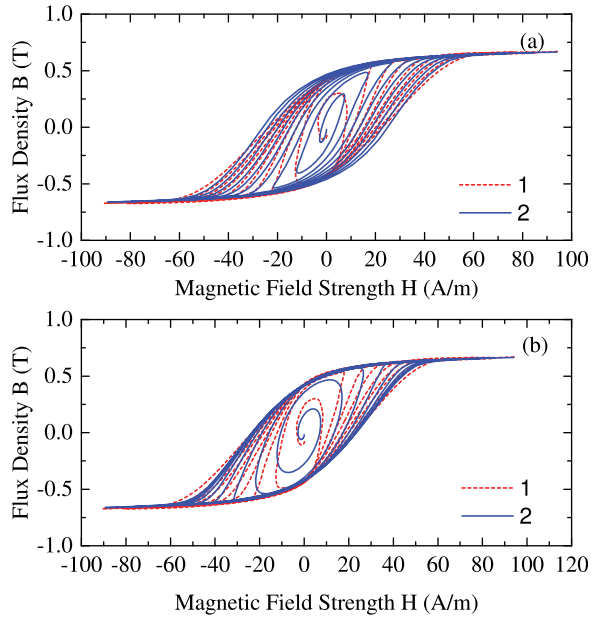

FIG. 8. Measured (curve 1) and calculated (curve 2) equilibration curves using the phase shift model: (a) with constant φ; (b) with time dependent φ. The fitted parameters are $\mu_{max} = 40\,000$, $\mu_0 M_s = 0.73\,\mathrm{T}$, $\varphi = 21°$, $v_3 = -13\mu_{max}\,\mathrm{T}^{-6}$, $v_4 = -30\mu_{max}\,\mathrm{T}^{-8}$, $v_5 = 42\mu_{max}\,\mathrm{T}^{-10}$, $v_6 = 15\mu_{max}\,\mathrm{T}^{-12}$, $c_1 = 0.9\,\mathrm{s}^{-1}$, $c_2 = 1.3\,\mathrm{s}^{-2}$.

To measure the equilibration curves of the sample, a 10-turn primary coil and a 50-turn secondary coil were wrapped toroidally around the sample. The equilibration field (10 cycles, 10 Hz, linear decreasing H) was initiated by a current through the primary coil. The flux density was calculated by integration of the induced voltage in the secondary coil. In order to avoid environmental disturbances, the sample was placed in the MSR at TUM which had a residual field less than 1 nT. Figs. 7 and 8 show the measured and simulated equilibration curves of the cylindrical sample. Before the equilibration began, 5 preceding cycles with the same amplitude (not shown) were used in the experiment to achieve reproducible and stable initial conditions. Fig. 7(b) illustrates that the simulated flux matched the experimental flux in time. Note that the predicted residual flux at the end of the equilibration (t = 1 s) is verified in Fig. 7(b).

TABLE I. Quality of simulations.

Simulation	NRMSD (%)	R^2
JA model	4.77	0.9762
Phase shift model with constant φ	9.74	0.9336
Phase shift model with time-dependent φ	6.44	0.9710

The normalized root mean square deviation (*NRMSD*) is calculated to show the differences between values predicted by models and the values actually observed. The coefficient of determination denoted R^2 also provides a measure of how well observed outcomes are predicted by the models.[18] The *NRMSD* and the R^2 of the equilibration simulations are shown in Table I. The statistical analysis demonstrates that both simulation methods are in good agreement with the experimental data and that the simulation based on the JA model provided better accuracy than the phase shift model.

The numerical calculations can also be applied to more complex geometries. An example, as shown in Fig. 6(b), was cut from a permalloy sheet and was formed as a closed magnetic path with constant cross section. The cylindrical sample and the snake sample were made of the same kind of permalloy, thus the simulations use the same parameters. After equilibration, the flux density was measured at 8.5 cm above the sample in the MSR at TUM. The maximum magnitude of the measured flux density was 5.16 ± 0.05 nT. The observed magnetic field distributions match the simulations as shown in Fig. 9. The computation time for this complex snake geometry using the phase shift model was 16 h, while the JA Model needed 18 h, running in COMSOL 5.1 on a computer with a 3.2 GHz central processing unit (CPU) and 40 GB of Random-access memory (RAM).

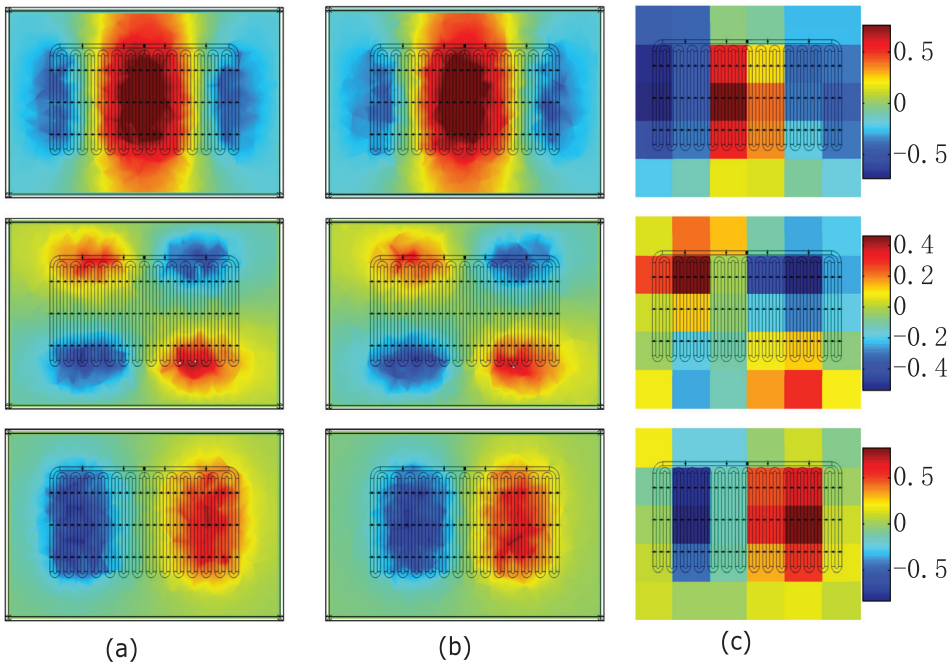

FIG. 9. The lines are the relative amount $\frac{\vec{B}}{|B|_{max}}$ of B_x, B_y, B_z; The columns are (a) calculated based on JA model; (b) calculated by phase shift model; and (c) measured in experiment.

V. CONCLUSION

Two numerical methods to calculate the behavior of 3D permalloy structures during equilibration were developed and tested against experiment. Both models can calculate equilibration in background fields, which is necessary for EDM and low field NMR experiments. The large-scale simulations for MSRs will need considerable computer power because of the tracing of the space- and time-dependent magnetic field during the whole process. The phase shift model was specifically tailored for faster computation, but it resulted in relatively small performance gains.

The models for small objects already help us to understand the theoretical principles and fundamental problems of equilibration. The intuitive optimization of the main equilibration parameters used hitherto can now be replaced by an optimization based on the proposed calculation methods. This work provides a basis for improved modelling of residual fields and their temporal stability inside complex geometries of magnetizable materials, in particular, for MSRs.

ACKNOWLEDGMENTS

This work was supported by DFG Priority Program SPP 1491, the Cluster of Excellence "Origin and Structure of the Universe," National Natural Science Foundation of China with No. 51407048, and the Fundamental Research Funds for the Central Universities with No. HIT.NSRIF.201664. We gratefully acknowledge IMEDCO AG for providing the material samples.

[1]I. Altarev, S. Chesnevskaya *et al.*, "A next generation measurement of the electric dipole moment of the neutron at the FRM II," Nuovo Cimento C **35**, 122 (2012).
[2]F. Allmendinger, W. Heil *et al.*, "New limit on Lorentz-invariance- and CPT-violating neutron spin interactions using a free-spin-precession ^{3}He-^{129}Xe comagnetometer," Phys. Rev. Lett. **112**, 110801 (2014).
[3]N. F. Ramsey, "Electric-dipole moments of particles," Annu. Rev. Nucl. Part. Sci. **32**, 211 (1982).
[4]N. F. Ramsey, "Experiments with separated oscillatory fields and hydrogen masers," Rev. Mod. Phys. **62**, 541 (1990).
[5]J. Pendlebury, S. Afach *et al.*, "Revised experimental upper limit on the electric dipole moment of the neutron," Phys. Rev. D **92**, 092003 (2015).
[6]M. Burghoff, T. H. Sander *et al.*, "DC magnetoencephalography: Direct measurement in a magnetically extremely-well shielded room," Appl. Phys. Lett. **85**, 6278 (2004).
[7]J. Bork, H. Hahlbohm *et al.*, "The 8-layered magnetically shielded room of the PTB: Design and construction," in *Proceedings of the 12th International Conference on Biomagnetism*, 2001, pp. 970–973.
[8]I. Altarev, E. Babcock *et al.*, "A magnetically shielded room with ultra low residual field and gradient," Rev. Sci. Instrum. **85**, 075106 (2014).
[9]I. Altarev, M. Bales *et al.*, "A large-scale magnetic shield with 10^6 damping at millihertz frequencies," J. Appl. Phys. **117**, 183903 (2015).
[10]F. Thiel, A. Schnabel *et al.*, "Demagnetization of magnetically shielded rooms," Rev. Sci. Instrum. **78**, 035106 (2007).
[11]I. Altarev, P. Fierlinger *et al.*, "Minimizing magnetic fields for precision experiments," J. Appl. Phys. **117**, 233903 (2015).
[12]D. C. Jiles and D. L. Atherton, "Theory of ferromagnetic hysteresis (invited)," J. Appl. Phys. **55**, 2115 (1984).
[13]D. C. Jiles and D. L. Atherton, "Theory of ferromagnetic hysteresis," J. Magn. Magn. Mater. **61**, 48–60 (1986).
[14]D. C. Jiles and D. L. Atherton, "Correction," J. Magn. Magn. Mater. **92**, 289 (1990).
[15]D. C. Jiles, "Frequency dependence of hysteresis curves in conducting magnetic materials," J. Appl. Phys. **76**, 5849 (1994).
[16]D. C. Jiles, "Erratum: "Frequency dependence of hysteresis curves in conducting magnetic materials" [J. Appl. Phys. **76**, 5849 (1994)]," J. Appl. Phys. **77**, 4834 (1995).
[17]A. Bergqvist, "A simple vector generalization of the Jiles-Atherton model of hysteresis," IEEE Trans. Magn. **32**, 4213–4215 (1996).
[18]R. Anderson-Sprecher, "Model comparisons and R^2," Am. Stat. **48**, 113–117 (1994).